

Effective Field Theory for Dilute Fermi Systems

H.-W. Hammer* and R. J. Furnstahl†

Department of Physics

The Ohio State University, Columbus, OH 43210

(April 18, 2000)

Abstract

The virtues of an effective field theory (EFT) approach to many-body problems are illustrated by deriving the expansion for the energy of an homogeneous, interacting Fermi gas at low density and zero temperature. A renormalization scheme based on dimensional regularization with minimal subtraction leads to a more transparent power-counting procedure and diagrammatic expansion than conventional many-body approaches. Coefficients of terms in the expansion with logarithms of the Fermi momentum are determined by the renormalization properties of the EFT that describes few-body scattering. Lessons for an EFT treatment of nuclear matter are discussed.

PACS number(s): 05.30.Fk, 07.10.Ca, 11.10.Hi, 21.65.+f

Typeset using REVTeX

*hammer@mps.ohio-state.edu

†furnstahl.1@osu.edu

I. INTRODUCTION

The effective field theory (EFT) approach exploits the separation of scales in physical systems [1–5]. The application of EFT methods to many-body problems promises insight into the analytic structure of observables and a consistent organization of many-body corrections, with reliable error estimates. Our ultimate goal is to calculate the properties of nuclear matter and finite nuclei, but there are many issues as yet unresolved concerning the practical application of EFT methods to these systems. As a step toward this goal, we consider a simpler problem for which we can illustrate some essential features that might be obscured in the full nuclear matter treatment.

The dilute Fermi gas has often served as a benchmark many-body problem, despite a shortage of physical applications. Recently, there has been experimental progress in creating and measuring dilute low-temperature Fermi systems [6], although these experiments at present are not sensitive to interactions. In this paper, we consider a uniform system of nonrelativistic fermions of mass M , interacting via a purely repulsive, spin-independent underlying interaction with characteristic range $R \equiv 1/\Lambda$. The restriction to repulsive interactions allows us to postpone discussion of Cooper pair and liquid-gas instabilities [7].

The prototype interaction of this type is a hard-sphere repulsion of radius R . For momenta $p \ll \Lambda = 1/R$, two-body scattering with a hard-sphere potential is described by the effective range expansion [see Eq. (3)]. All of the effective range parameters are “natural”; that is, their magnitude is given by a power of the underlying scale R times a dimensionless number of order unity. For general interactions, natural values are expected for the effective range and higher-order parameters, but not necessarily for the scattering length, which can be arbitrarily large if there is a bound state near zero energy. The latter case is of particular interest, of course, because of the nature of s -wave nucleon-nucleon scattering. However, a fine-tuned scattering length requires special treatment [4,5], so our discussion here will assume natural scattering lengths.

To our knowledge, the most complete low-density expansion for the ground-state energy per particle of such a system in the literature is [8–10]:

$$\begin{aligned} \frac{E}{N} = \frac{k_F^2}{2M} & \left[\frac{3}{5} + (g-1) \left\{ \frac{2}{3\pi} (k_F a_s) + \frac{4}{35\pi^2} (11 - 2 \ln 2) (k_F a_s)^2 + \frac{1}{10\pi} (k_F r_s) (k_F a_s)^2 \right. \right. \\ & + (0.076 + 0.057(g-3)) (k_F a_s)^3 \Big\} + (g+1) \frac{1}{5\pi} (k_F a_p)^3 \\ & \left. \left. + (g-1)(g-2) \frac{16}{27\pi^3} (4\pi - 3\sqrt{3}) (k_F a_s)^4 \ln(k_F a_s) + \dots \right] . \right. \end{aligned} \quad (1)$$

In Eq. (1), a_s and r_s are the s -wave scattering length and effective range, and a_p is the p -wave scattering length. The spin degeneracy is denoted by g . For a natural system, this is an expansion in Fermi momentum k_F over the scale Λ . The mean-field correction of $\mathcal{O}(k_F^3)$ dates from 1929 [11], the $\mathcal{O}(k_F^4)$ correction from the fifties [12], while the $\mathcal{O}(k_F^5)$ correction and the logarithm were found in the sixties [13]. The complete expression in Eq. (1) has been derived using the method of correlation functions [8], by expanding Goldstone diagrams [9,10], and by expanding Feynman diagrams [10]. Here we rederive and illuminate this result using EFT methods.

While field theory approaches to many-body physics are well-established (e.g., Refs. [13] and [14]), the treatment of divergences and renormalization issues for a dilute Fermi system

[8–10] are reminiscent of the old-style approach to renormalization theory, in which renormalization is primarily a technical device to get rid of divergences in perturbation theory (i.e., to sweep problems under the rug) [15]. The modern viewpoint in particle physics that “renormalization is an expression of the variation of the structure of physical interactions with changes in the scale of the phenomena being probed” [15] has led to powerful and elegant renormalization group methods and to the development of the effective field theory approach, which provides low-energy descriptions in terms of local, nonrenormalizable interactions.

We want to revisit the dilute Fermi gas with the same type of insight that effective field theory has given to particle physics. Some first steps were taken in Ref. [16], in which a double expansion in momentum and the strength of a model potential was exploited to study renormalization and EFT breakdown at finite density. Here we extend the analysis to a general low-density expansion that is perturbative only in the Fermi momentum.

Effective field theories for free-space scattering of two fermions are now well understood [4,5] and are particularly straightforward for systems with natural scattering lengths [17]. At low energies, with momentum $k \ll \Lambda$, the underlying interactions are not resolved, so they may be replaced by a series of local (contact) interactions; this description is completely general to the order of truncation. Contributions to the scattering amplitude are expressed as a systematic diagrammatic expansion in k/Λ . The prescription for determining what diagrams contribute to a given order in the expansion is called power counting. Since the contact interactions are highly singular, they require regularization and renormalization, and the power counting prescription depends on the subtraction scheme. It is particularly useful to have a subtraction scheme in which any Feynman graph with a particular vertex only contributes to the expansion of the amplitude at a particular order, and for which power counting is simple dimensional analysis. For a natural system, these conditions are satisfied by minimal subtraction implemented using dimensional regularization [17].

The EFT expansion for free-space two-body scattering efficiently reproduces the effective range expansion, which is a Taylor expansion in external momentum p divided by the characteristic scale of the underlying interaction Λ . When using a low resolution probe, only the scale Λ of new, unresolved physics enters. Up to factors of order unity, the radius of convergence of the expansion (i.e., where errors are under control) is Λ , even though the domain of analyticity may be infinite. A reliable estimate for the truncation error is order unity times k/Λ to the first omitted power.

For a problem like this where the physics is “transparent”, the calculation would ideally be equally transparent. The free-space EFT treatment does exactly that. One might expect a simple analysis to be possible at finite density as well, but the standard treatments are actually quite complicated, with summations to all orders and expansions for each diagram [9,10]. The EFT approach presented here maintains the virtues of the free-space EFT description: each Feynman diagram contributes to a definite order in the k_F/Λ expansion of the energy. Previous work strained to eliminate divergences; with an EFT they are natural and understood and even exploited.

The analytic structure of the low-density expansion as a function of k_F is dictated by the interplay of short- and long-distance behavior. This is particularly well manifested in the effective field theory approach. In a recent paper, Braaten and Nieto [18] showed how renormalization effects in a dilute *boson* gas determine the coefficients of logarithms in the

low-density expansion of the energy. Here we make an analogous analysis for fermion systems to find the coefficient of the logarithm in Eq. (1) from renormalization group arguments. Extensions of this analysis may be fruitful in deriving the analytic structure of the energy functional of nuclear matter and other strongly interacting fermion systems. We also discuss how to complete the renormalization, which *requires* additional input beyond what is determined by two-body scattering.

In section II, we review how EFT power counting in free space generates the effective range expansion. In section III, the EFT is used to reproduce the analytic terms in Eq. (1) and in section IV the logarithm is discussed. We focus on the physics with a minimum of formalism. More complete details will be given elsewhere, including numerical details and extensions to finite temperature and other observables [7]. The results are put in the context of the nuclear matter problem in Section V.

II. FREE-SPACE EFT

In this section, we review the EFT for two-body scattering in free space.¹ We consider a natural EFT for heavy nonrelativistic fermions of mass M , whose interactions are spin-independent and with strength correctly estimated by naive dimensional analysis based on an underlying scale Λ . In the center of momentum frame, the scattering amplitude T of two particles with momenta of magnitude k and scattering angle θ can be expanded in partial waves as

$$T(k, \cos \theta) = \frac{4\pi}{M} \sum_l \frac{2l+1}{k \cot \delta_l - ik} P_l(\cos \theta) , \quad (2)$$

where δ_l is the scattering phase shift for angular momentum l and P_l is a Legendre polynomial. Furthermore, for short-range interactions $k \cot \delta_l$ can be expanded in powers of k^2 as

$$k \cot \delta_0 = -\frac{1}{a_s} + \frac{1}{2} r_s k^2 + \dots , \quad k \cot \delta_1 = -\frac{3}{k^2 a_p^3} + \dots , \quad (3)$$

where a_s , a_p , and r_s are the s - and p -wave scattering lengths and s -wave effective range, respectively. Inserting Eq. (3) into Eq. (2) and expanding the result up to $\mathcal{O}(k^2/\Lambda^2)$, we obtain

$$T(k, \cos \theta) = -\frac{4\pi a_s}{M} \left[1 - ia_s k + (a_s r_s/2 - a_s^2) k^2 \right] - \frac{4\pi a_p^3}{M} k^2 \cos \theta + \mathcal{O}(k^3/\Lambda^3) . \quad (4)$$

For a natural system, $a_s \sim a_p \sim r_s \sim 1/\Lambda \equiv R$ and we have a *perturbative* expansion in k/Λ . An example commonly studied is a hard-sphere gas with radius R , in which case $a_s = a_p = R$ and $r_s = 2R/3$.

Since we assume $k \ll \Lambda$, all interactions in the EFT are short-ranged and we have only contact interactions. Thus to reproduce this expansion with an EFT we consider a general

¹For a more complete treatment, see Refs. [17,19].

local Lagrangian for a nonrelativistic fermion field that is invariant under Galilean, parity, and time-reversal transformations:²

$$\begin{aligned}\mathcal{L} = & \psi^\dagger \left[i\partial_t + \frac{\vec{\nabla}^2}{2M} \right] \psi - \frac{C_0}{2} (\psi^\dagger \psi)^2 + \frac{C_2}{16} \left[(\psi \psi)^\dagger (\psi \vec{\nabla}^2 \psi) + \text{h.c.} \right] \\ & + \frac{C'_2}{16} \left[2(\psi^\dagger \vec{\nabla}^2 \psi) \psi^\dagger \psi - (\psi \vec{\nabla}^2 \psi)^\dagger \psi \psi + \text{h.c.} \right] \\ & - \frac{D_0}{6} (\psi^\dagger \psi)^3 + \dots,\end{aligned}\tag{5}$$

where $\vec{\nabla} = \vec{\nabla} - \vec{\nabla}$ is the Galilean invariant derivative and h.c. denotes the hermitian conjugate. The dots represent terms with more derivatives and/or more fields. Higher-order terms with time derivatives are omitted, as they can be eliminated in favor of terms with spatial derivatives [17]. Relativistic corrections can be included systematically, but all such terms are suppressed by factors of $(\Lambda/M)^2$, which we take to be negligible; they are considered explicitly in Ref. [7].

The S-matrix for the scattering of free fermions is simply related to a sum of Feynman graphs computed according to this Lagrangian. The terms in Eq. (5) involving only four fermion fields reduce in momentum space to simple polynomial vertices that are equivalent to a momentum expansion of an EFT potential for particle-particle scattering,

$$\langle \mathbf{k}' | V_{EFT} | \mathbf{k} \rangle = C_0 + C_2(\mathbf{k}^2 + \mathbf{k}'^2)/2 + C'_2 \mathbf{k}' \cdot \mathbf{k} + \dots,\tag{6}$$

(see Fig. 1 for the Feynman rules). Because of Galilean invariance, the interaction depends only on the relative momenta \mathbf{k} and \mathbf{k}' of the incoming and outgoing particles. The coefficients C_0 , C_2 , and C'_2 can be obtained from matching the EFT to a more fundamental theory or to (at least) three independent pieces of experimental data. It is important to note that Eq. (6) is *not* simply the term-by-term momentum-space expansion of an underlying potential because the coefficients also contain short-distance contributions from loop graphs (see Ref. [16] for a simple example of the matching and renormalization of the coefficients).

The loop integrals that appear in Feynman graphs for two-body scattering with this EFT in D spatial dimensions reduce to

$$L_n \equiv \int \frac{d^D q}{(2\pi)^D} \frac{q^{2n}}{k^2 - q^2 + i\epsilon}.\tag{7}$$

For $D = 3$ spatial dimensions, these integrals are divergent and must be regulated. If we apply a sharp momentum cutoff Λ_c on q , evaluate the integral and expand in k , we find the leading terms have positive powers of Λ_c . These are called power divergences. For example, when $n = 0$,

$$L_0 \xrightarrow{D=3} -\frac{1}{2\pi^2} \Lambda_c - \frac{i}{4\pi} k + \mathcal{O}(k^2/\Lambda_c).\tag{8}$$

²The extension to spin- and/or isospin-dependent interactions is straightforward and is illustrated in Ref. [7].

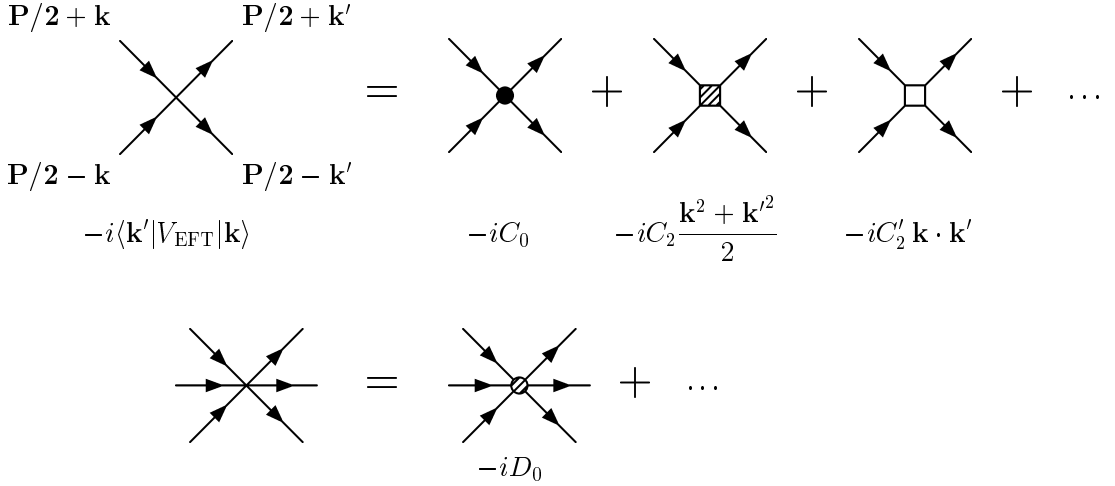


FIG. 1. Feynman rules for $\langle \mathbf{k}' | V_{\text{EFT}} | \mathbf{k} \rangle$ and the leading 3-body contact interaction. The spin indices have been suppressed.

The power divergences come from the short-distance region of the integral where the loop momentum is of order Λ_c . This contribution is incorrect and depends on the details of how we regulate the integral, but can be removed systematically using local counterterms. In contrast, contributions from loop momenta of order of the small external momentum k [the second term in Eq. (8)] are physical. These contributions are completely decoupled; the Λ_c coefficient tells us nothing about the k coefficient.

If we imagine two-body scattering in $D = 2$ dimensions, the situation is different, because there will always be a logarithmic divergence (as well as power divergences in general). For example, when $n = 0$,

$$L_0 \xrightarrow{D=2} \frac{1}{2\pi} \ln(k/\Lambda_c) + \mathcal{O}(1) . \quad (9)$$

The dependence on $\ln(\Lambda_c)$ is canceled by a counterterm, but now the contributions from the different momentum regions are coupled. Since the logarithms of k and Λ_c must match, the coefficient of the logarithm is independent of the regularization. Further, it can be determined by looking only at the log divergence in the integral, without a full calculation. We will take advantage of this simplification later when we consider three-body scattering, in which logarithmic divergences appear for $D = 3$.

Since the power divergences do not provide useful information here and complicate the power counting, it is appropriate to use a minimal subtraction scheme, which by construction subtracts the power divergences. Dimensional regularization with minimal subtraction is particularly convenient for a natural EFT, since loop integrals for two-body scattering pick up *only* the scale of the external momentum (logarithms are also possible when more than two fermions scatter). In particular, [17]

$$L_n \xrightarrow{D=3} -\frac{i}{4\pi} k^{2n+1} . \quad (10)$$

Thus, the underlying physical scale Λ appears only in the coefficients and the loops contribute only factors of k , which can be determined by dimensional analysis.

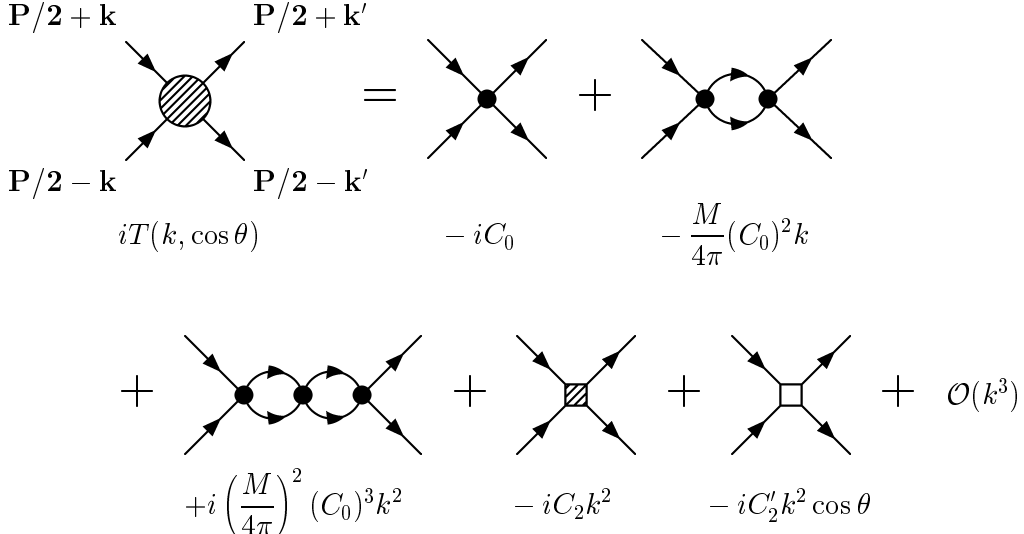


FIG. 2. Expansion of $T(k, \cos \theta)$ in the EFT.

Therefore the estimated contribution of a given diagram is found by counting (i) for every propagator a factor M/k^2 , (ii) for every loop integration a factor of k^5/M , and (iii) for every n -body vertex with $2i$ derivatives a factor $k^{2i}/M\Lambda^{2i+3n-5}$. This scaling of the coefficients with M and Λ follows from Galilean invariance and dimensional analysis [17]. In particular, the vertices with four and six fields scale as

$$C_{2i} \sim \frac{4\pi}{M\Lambda^{2i+1}} \quad \text{and} \quad D_{2i} \sim \frac{4\pi}{M\Lambda^{2i+4}}, \quad (11)$$

which means that more complicated graphs are suppressed at low energies by additional powers of k/Λ . As above, Λ is an ultraviolet scale which is determined by the physics not explicitly included in the EFT (such as the mass of a heavy exchanged particle). For momenta $k \sim \Lambda$, the expansion in powers of k/Λ breaks down and the new physics at the scale Λ has to be explicitly included in the EFT. Therefore, Λ is also called the breakdown scale of the EFT.

We can use the topological properties of a graph to determine that a diagram with L loops or E external lines and V_{2i}^n n -body vertices with $2i$ derivatives scales precisely as k^ν , where

$$\begin{aligned} \nu &= 3L + 2 + \sum_{n=2}^{\infty} \sum_{i=0}^{\infty} (2i - 2)V_{2i}^n \\ &= 5 - \frac{3}{2}E + \sum_{n=2}^{\infty} \sum_{i=0}^{\infty} (2i + 3n - 5)V_{2i}^n. \end{aligned} \quad (12)$$

At every order in k/Λ there are a finite number of graphs that contribute.

Now we can determine the coefficients C_{2i} by matching. In our case, the experimental data we match to are the leading coefficients of the effective range expansion for the scattering amplitude T , Eq. (4). Evaluating T in the center-of-momentum frame of the two particles, we obtain (see Fig. 2)

$$T(k, \cos \theta) = -C_0 \left[1 - i \frac{M}{4\pi} C_0 k + \frac{C_2}{C_0} k^2 - \left(\frac{M}{4\pi} C_0 \right)^2 k^2 + \frac{C'_2}{C_0} k^2 \cos \theta \right] + \mathcal{O}(k^3/\Lambda^3), \quad (13)$$

where $|\mathbf{k}| = |\mathbf{k}'| = k$ and θ is the scattering angle. Matching Eq. (13) to Eq. (4), we can express the C_{2i} in terms of the effective range parameters:

$$C_0 = \frac{4\pi a_s}{M}, \quad C_2 = C_0 \frac{a_s r_s}{2}, \quad \text{and} \quad C'_2 = \frac{4\pi a_p^3}{M}. \quad (14)$$

Thus the EFT reproduces the effective range expansion in free space.³ With the interaction parameters in the Lagrangian expressed in terms of the effective range parameters, we are now ready to apply the EFT to systems at finite density.

III. DILUTE FERMI SYSTEMS

We first review the noninteracting Fermi gas at zero temperature to set our notation and conventions. In this case, all states up to the Fermi momentum k_F are occupied while the ones above k_F are empty. The density $\rho = N/V$ of a system with Fermi momentum k_F and degeneracy $g = (2s + 1)$ is obtained by summing over all occupied states,

$$\rho = g \int \frac{d^3 k}{(2\pi)^3} \theta(k_F - k) = \frac{g k_F^3}{6\pi^2}. \quad (15)$$

The energy density \mathcal{E}_0 of a noninteracting Fermi gas is given by weighting the integral in Eq. (15) with the free single particle energy $\omega_{\mathbf{k}} \equiv \mathbf{k}^2/(2M)$, which leads to

$$\mathcal{E}_0 = \rho \frac{3}{5} \frac{k_F^2}{2M}. \quad (16)$$

The energy per particle E_0/N is simply \mathcal{E}_0/ρ .

Equation (16) receives corrections from the interaction between the fermions. For low-density systems with short-range interactions, $\rho \propto k_F^3 \ll 1/R^3 \sim \Lambda^3$, and the bulk properties of the system are amenable to an expansion in $k_F R$ or k_F/Λ . As discussed earlier, the EFT method is ideally suited to deal with such a separation of scales. In this section, we present an EFT for low-density Fermi systems and illustrate its application by calculating the corrections to Eq. (16) to order $(k_F R)^3$. The use of contact interactions and EFT power counting makes the EFT treatment straightforward and more transparent than traditional approaches (*e.g.*, see Ref. [8]).

The ground-state energy density \mathcal{E} can be expressed as a sum of Hugenholtz diagrams, which are closed, connected Feynman diagrams with appropriate symmetry factors (see Fig. 3). To apply the EFT from the previous section at finite density, we have to adapt the

³If the scattering length is unnatural, the power counting has to be modified and the perturbation series must be resummed to avoid a premature breakdown of the EFT. This case has received considerable attention recently [4,5].

power-counting rules from free space to the medium. This is immediate with dimensional regularization and minimal subtraction, because the typical momentum flowing in *both* particle and hole lines in energy diagrams is of order k_F (see below). The result is clear for hole lines, but particle lines can in principle have momenta that are unbounded or as large as an imposed cutoff Λ_c . However, as discussed above, the contributions of states with momenta close to the cutoff, which depends on the regularization scheme in an EFT, are removed by minimal subtraction. The correct effect of high-momentum modes on low-energy physics is incorporated in the coefficients of the local operators in the Lagrangian instead. The end result is that we can use Feynman diagrams for the ground state energy, in which holes and particles are propagated together, and apply the free-space power counting with k_F playing the role of external momentum.

Thus we estimate the contribution of a given Hugenholtz diagram by counting (i) for every propagator a factor M/k_F^2 , (ii) for every loop integration a factor of k_F^5/M , and (iii) for every n -body vertex with $2i$ derivatives a factor $k_F^{2i}/M\Lambda^{2i+3n-5}$. The mass M enters all Feynman diagrams in the same way as a factor $1/M$. Furthermore, the range R always has to match up with k_F to produce the dimensionless expansion parameter $k_F R$. The correct power of R can be inferred from the overall dimension of the diagram, which is an energy density. Consequently, it is sufficient to keep track of the powers of k_F to classify the relative size of diagrams. The power counting rules are conveniently summarized in one equation in terms of the vertices of a given diagram. In particular, a graph with V_{2i}^n n -body vertices with $2i$ derivatives scales as k_F^ν , where ν is given by

$$\nu = 5 + \sum_{n=2}^{\infty} \sum_{i=0}^{\infty} (2i + 3n - 5) V_{2i}^n \quad (17)$$

[this follows from Eq. (12) with $E = 0$]. As in free space, diagrams with more vertices and more derivatives are suppressed, and therefore the EFT expansion is efficient and systematic.

The leading order Hugenholtz diagrams contributing to the energy density are shown in Fig. 3. From Eq. (16), the energy density of the noninteracting Fermi gas is of $\mathcal{O}(k_F^5)$; the first correction Fig. 3(a) is of $\mathcal{O}(k_F^6)$. The Feynman rules for the contributions to the noninteracting energy density from the diagrams in Fig. 3 are essentially the same as in standard many-body treatments (e.g., see Ref. [13,14]), which we summarize here.

First, draw all distinct, fully connected diagrams contributing to a given order in k_F [as determined by Eq. (17)]. Distinct diagrams are those that cannot be deformed to coincide with each other, including the direction of arrows. To evaluate a diagram:

1. Assign nonrelativistic four-momenta (frequency and three-momentum) to all lines and enforce four-momentum conservation at each vertex.
2. For each vertex include a factor $-i$ times the corresponding term from the effective potential $\langle \mathbf{k}' | V_{\text{EFT}} | \mathbf{k} \rangle$, as shown in Fig. 1. (Recall that \mathbf{k} and \mathbf{k}' are *relative* momenta.) The spin structure of the vertices has been suppressed in Fig. 1. For spin-independent interactions, the two-body vertices have the structure $(\delta_{\alpha\gamma}\delta_{\beta\delta} + \delta_{\alpha\delta}\delta_{\beta\gamma})$, where α, β are the spin indices of the incoming lines and γ, δ are the spin indices of the outgoing lines. For spin-dependent interactions one inserts the appropriate operator in spin space at each vertex instead.

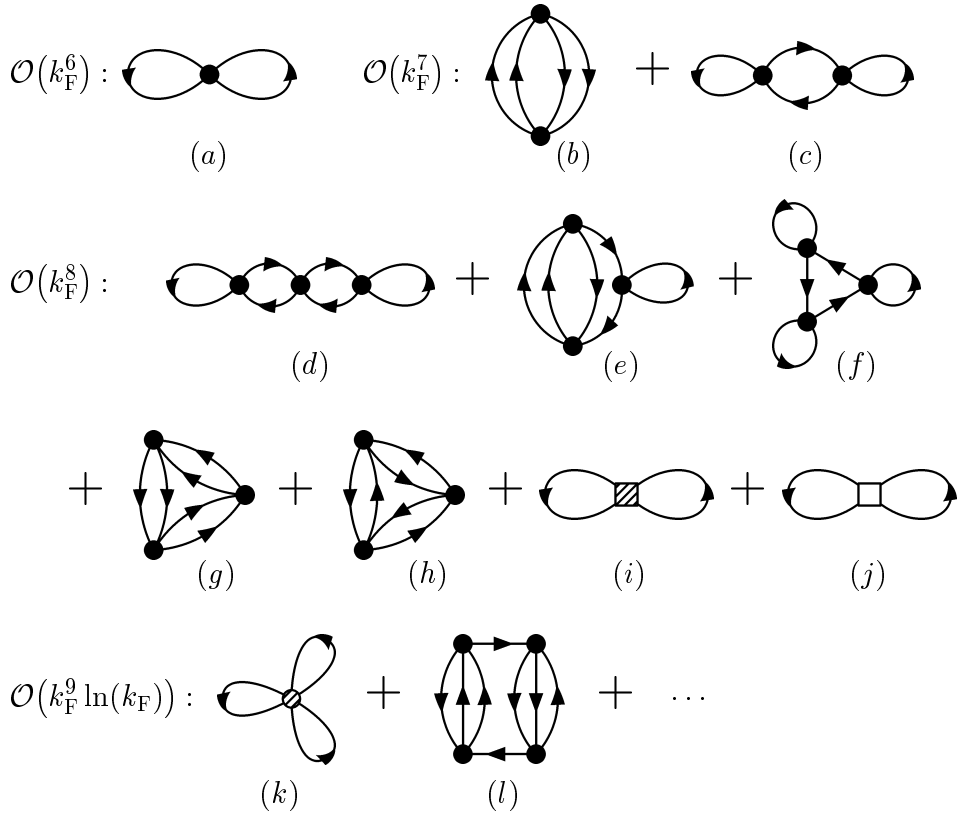


FIG. 3. Hugenholtz diagrams for the energy density \mathcal{E} in a homogeneous, dilute Fermi system. The vertices are defined in Fig. 1.

For each internal line include a factor $iG_0(\tilde{k})_{\alpha\gamma}$, where $\tilde{k} \equiv (k_0, \mathbf{k})$ is the four-momentum assigned to the line, α and γ are spin indices, and

$$iG_0(\tilde{k})_{\alpha\gamma} = i\delta_{\alpha\gamma} \left(\frac{\theta(k - k_F)}{k_0 - \omega_{\mathbf{k}} + i\epsilon} + \frac{\theta(k_F - k)}{k_0 - \omega_{\mathbf{k}} - i\epsilon} \right). \quad (18)$$

3. Perform the spin summations in the diagram. In every closed fermion loop, substitute $-g$ for each $\delta_{\alpha\alpha}$.
4. Integrate over all independent momenta with a factor $\int d^4k/(2\pi)^4$ where $d^4k \equiv dk_0 d^3k$. If the spatial integrals are divergent, they are defined in D spatial dimensions and renormalized using minimal subtraction as discussed in Sect. II and Ref. [17]. For lines ending and originating at the same vertex, multiply by $\exp(ik_0\eta)$ and take the limit $\eta \rightarrow 0^+$ after the contour integrals have been carried out. This procedure automatically takes into account that such lines can only be hole lines.
5. Multiply by a symmetry factor $i/(S \prod_{l=2}^{l_{\max}} (l!)^k)$ where S is the number of vertex permutations that transform the diagram into itself, and k is the number of equivalent

l -tuples of lines. Equivalent lines are lines that begin and end at the same vertices with the same direction of arrows.

We illustrate the use of these Feynman rules by applying them to some of the diagrams in Fig. 3. We start with the diagram at $\mathcal{O}(k_F^6)$, Fig. 3(a). This diagram has one vertex and one equivalent pair of lines originating and ending at this vertex. The overall factor is therefore $i/2$ and we have

$$\mathcal{E}_1 = \frac{i}{2} (-iC_0) g(g-1) \left(\lim_{\eta \rightarrow 0^+} \int \frac{d^4 k}{(2\pi)^4} e^{ik_0 \eta} iG_0(\tilde{k}) \right)^2, \quad (19)$$

The dk_0 integration is performed using contour integration, which picks up the $\theta(k_F - k)$ pole, and the remaining $d^3 k$ integral up to k_F is trivial. The result is

$$\mathcal{E}_1 = \rho(g-1) \frac{k_F^2}{2M} \frac{2}{3\pi} k_F a_s, \quad (20)$$

where Eqs. (14) and (15) have been used [11]. \mathcal{E}_1 is of order k_F^6 as expected from the power counting. We label the energy contributions labeled by the power of k_F that accompanies the generic scale R ; this power is indicated by the subscript j on \mathcal{E}_j .

At $\mathcal{O}(k_F^7)$ we have two diagrams. Figure 3(c) vanishes at $T = 0$ because it involves particle-hole pairs of equal momentum at the Fermi surface, which have no phase space available. (This leads to integrals of the form $\int dk f(k) \theta(k_F - k) \theta(k - k_F)$ that vanish if $f(k)$ is regular.) Such diagrams are called “anomalous.” Figure 3(b) has $S = 2$ and two equivalent pairs of lines. Applying the Feynman rules we obtain

$$\mathcal{E}_2 = -i \frac{(C_0)^2}{4} g(g-1) \int \frac{d^4 k}{(2\pi)^4} \int \frac{d^4 p}{(2\pi)^4} \int \frac{d^4 q}{(2\pi)^4} G_0(\tilde{p}) G_0(\tilde{p} - \tilde{q}) G_0(\tilde{k} + \tilde{q}) G_0(\tilde{k}). \quad (21)$$

The frequency integrals are again simple contour integrals. A transformation to dimensionless center-of-mass variables \mathbf{s} , \mathbf{t} , and \mathbf{u} using

$$\mathbf{p} = k_F(\mathbf{s} + \mathbf{t}), \quad \mathbf{k} = k_F(\mathbf{s} - \mathbf{t}), \quad \text{and} \quad \mathbf{q} = k_F(\mathbf{t} - \mathbf{u}) \quad (22)$$

leads to

$$\begin{aligned} \mathcal{E}_2 = \rho(g-1) \frac{k_F^2}{2M} (k_F a_s)^2 & \frac{48}{(2\pi)^5} \int d^3 s \int d^3 t \int d^3 u \theta(1 - |\mathbf{s} + \mathbf{t}|) \theta(1 - |\mathbf{s} - \mathbf{t}|) \\ & \times \theta(|\mathbf{s} + \mathbf{u}| - 1) \theta(|\mathbf{s} - \mathbf{u}| - 1) \frac{1}{t^2 - u^2 + i\epsilon}, \end{aligned} \quad (23)$$

where Eq. (14) has been used again.

The integral over u in Eq. (23) contains a linearly divergent term in $D = 3$ dimensions (putting back the factors of k_F):

$$\mathcal{P} \int_{k_F}^{\infty} \frac{d^D u}{t^2 - u^2} = \mathcal{P} \int_0^{\infty} \frac{d^D u}{t^2 - u^2} - \mathcal{P} \int_0^{k_F} \frac{d^D u}{t^2 - u^2}. \quad (24)$$

These are principal value integrals. When dimensionally regularized, the first term on the right-hand side has no pole in $1/(D - 3)$ and no imaginary part, so it vanishes by our

minimal subtraction prescription. In the conventional approach, one avoids such power-law divergences by eliminating the potential, which is implicitly assumed to be valid for arbitrarily high momenta, in favor of the scattering amplitude. This amounts to summing the “ladder” diagrams to all orders and expanding the result afterwards. The EFT deals with such power law divergences more directly by avoiding the assumption of an underlying potential. Power law divergences are simply subtracted out and the effect of high energy modes is captured in the coefficients of the terms in the effective potential. Renormalization theory assures us that this procedure is consistent and correct.

The second term in Eq. (24) is finite and the remaining integrals can be evaluated analytically after some judicious partial integrations (see Appendix C of Ref. [16] for details). The net result for the second-order contribution to the energy density is

$$\mathcal{E}_2 = \rho(g-1) \frac{k_F^2}{2M} (k_F a_s)^2 \frac{4}{35\pi^2} (11 - 2\ln 2), \quad (25)$$

which was first obtained by Huang and Yang [12].

At $\mathcal{O}(k_F^8)$, we have seven diagrams contributing to the energy density. Their evaluation from the Feynman rules is straightforward although somewhat tedious; we will not go through the calculations in detail here but only make some comments. Three of the diagrams, Figs. 3(d), 3(e), and 3(f), vanish when evaluated. This is immediately clear for Fig. 3(d), which vanishes due to the same phase space argument as the similar diagram at $\mathcal{O}(k_F^7)$. In Fig. 3(e), the contributions of hole and particle propagation in the line with the tadpole loop attached cancel exactly. This cancellation is manifest once the frequency integrals have been carried out. Figure 3(f) can again be seen to vanish without any calculation. Assign a four-momentum \tilde{k} to the center loop to which the three tadpole loops are attached and perform the dk_0 integration. We have to evaluate $\int dk_0 G(\tilde{k})^3$, but only simple poles in k_0 contribute to the integral. The terms with simple poles, however, involve a factor $\theta(k - k_F)\theta(k_F - k)$ times a regular function and so the diagram vanishes. Note that because the interactions are contact terms, in general a large number of exchange diagrams vanish as anomalous diagrams.

Diagrams 3(g) and (h), each with three C_0 vertices, can be directly calculated. The first one contains a linear divergence similar to the diagram at $\mathcal{O}(k_F^7)$, which can be isolated (e.g., by transforming to center-of-mass variables), and then removed by minimal subtraction. The second diagram is finite. The integrals, however, cannot be evaluated analytically. We have calculated these integrals using Monte Carlo integration and reproduced the values given in the literature [8–10]. Numerical details will be discussed elsewhere [7].

Finally, there are diagrams 3(i) and 3(j), which contain C_2 and C'_2 vertices. These vertices contribute for the first time at $\mathcal{O}(k_F^8)$ and introduce a dependence on the s -wave effective range r_s and the p -wave scattering length a_p . The diagrams are very similar to the one at $\mathcal{O}(k_F^6)$ and can be evaluated directly. One must be careful with the sign of the relative momenta \mathbf{k} and \mathbf{k}' , since in the crossed contribution \mathbf{k}' changes its sign. This is irrelevant for the C_2 vertex, but for C'_2 it changes the overall factor $(g-1)$ into $(g+1)$. Adding all contributions at $\mathcal{O}(k_F^8)$, we have

$$\begin{aligned} \mathcal{E}_3 = \rho \frac{k_F^2}{2M} & \left[(g-1) \frac{1}{10\pi} (k_F a_s)^2 k_F r_s + (g+1) \frac{1}{5\pi} (k_F a_p)^3 \right. \\ & \left. + (g-1) \{ (0.07550 \pm 0.00003) + (g-3) (0.05741 \pm 0.00002) \} (k_F a_s)^3 \right], \end{aligned} \quad (26)$$

which agrees with previous calculations [8–10].

Equation (26) illustrates that the conventional hole-line expansion does not apply to the EFT-based diagrammatic expansion. Consider diagrams 3(g) and 3(h) again. Diagram 3(g) has 2-hole–4-particle and 4-hole–2-particle intermediate states while the diagram 3(h) has only 3-hole–3-particle intermediate states and should be relatively suppressed according to the hole-line expansion argument. Equation (26) shows that both diagrams are of the same order of magnitude, as expected from EFT power counting. We return to this point in the discussion below.

In this section we have calculated the energy density of a dilute Fermi gas up to order $(k_F R)^3$. In contrast to conventional calculations, the EFT approach is completely transparent and easily extended to higher orders, finite temperatures, and other observables. The EFT method is particularly advantageous when logarithmic divergences are present, as discussed in the next section.

IV. LOGARITHMIC SINGULARITIES

A naive extrapolation of Eq. (26) might lead one to conclude that the energy density has an analytic expansion in k_F/Λ . This would be true if the Feynman graphs contained only power divergences. However, diagrams for three-to-three scattering have logarithmic divergences and a consequence is that some terms in the energy density appear multiplied by powers of $\ln k_F$. Renormalization group methods provide a powerful tool to discern this analytic structure. We follow the discussion of Braaten and Nieto, who performed an analogous analysis for dilute Bose gases [18].

As we discussed in Sect. II, logarithmic divergences are special because they match onto logarithms of physical quantities. This means that we can identify where physical logarithms might appear by examining the renormalization group equations for the EFT coefficients. The general structure of these equations for dimensional regularization with minimal subtraction is

$$\mu \frac{d}{d\mu} g_j(\mu) = \beta_j(g) , \quad (27)$$

where μ is the (arbitrary) renormalization scale, g_j is a generic n -body coupling (e.g., a C_{2i} or a D_{2i}), and $\beta_j(g)$ is a polynomial in the couplings g_i with Λ -independent coefficients. The terms in the polynomial correspond to diagrams which, if they have logarithmic divergences, will have nonzero coefficients. Matching Λ dimensions on each side of the equation [recall Eq. (11)] greatly restricts the possible terms [20].

The running of two-body couplings C_{2i} is determined by graphs in the two-body sector where there are only power divergences; therefore, none of these couplings depend on μ . So the lowest-dimension coupling that might run is D_0 , the coefficient of the three-body contact term in the free EFT Lagrangian,

$$\mathcal{L}_{\text{3-body}} = -\frac{1}{6} D_0 (\psi^\dagger \psi)^3 . \quad (28)$$

Since $D_0 \sim 1/M\Lambda^4$ and $C_{2i} \sim 1/M\Lambda^{2i+1}$, β_j could have four C_0 ’s or one C_0 and one C_2 or C'_2 . The latter two correspond to finite tree diagrams, so their coefficients in β_j are zero.

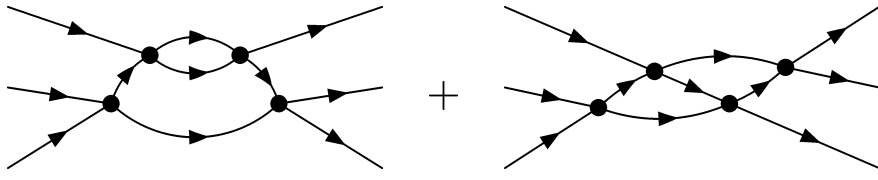


FIG. 4. Diagrams for three-particle scattering in free space that contribute to the running of D_0 .

That leaves only 2-loop diagrams with four C_0 vertices, and an inspection of these uncovers logarithmic divergences in the diagrams in Fig. 4.

Performing the loop integrals in $D < 3$ dimensions and then analytically continuing back to $D = 3$, the logarithmic divergences leads to simple poles $1/(D-3)$ in the $3 \rightarrow 3$ scattering amplitude. Braaten and Nieto [18] have extracted the pole part of the diagrams in Fig. 4 (which involves removing an overlapping divergence). Using their result and taking into account the diagrams with cyclic permutations of the external momenta, the pole part of the $3 \rightarrow 3$ scattering amplitude is

$$\begin{aligned} i[\mathcal{T}_{3 \rightarrow 3}]_{\text{pole}} &= -iM^3 (C_0)^4 \frac{4\pi - 3\sqrt{3}}{8\pi^3} \frac{1}{D-3} \mu^{2(3-D)} \\ &= -iM^3 (C_0)^4 \frac{4\pi - 3\sqrt{3}}{8\pi^3} \left[\frac{1}{D-3} - 2 \ln \mu + \dots \right], \end{aligned} \quad (29)$$

where the spin structure has been suppressed and the omitted terms vanish as $D \rightarrow 3$. A counterterm removes the $1/(D-3)$ pole in Eq. (29), leaving a finite term $[\mathcal{T}_{3 \rightarrow 3}]_{\text{finite}}$, which depends on the arbitrary scale μ . Since physical quantities cannot depend on μ , the renormalized coupling D_0 must satisfy

$$\frac{d}{d\mu} (i[\mathcal{T}_{3 \rightarrow 3}]_{\text{finite}} - iD_0) = 0, \quad (30)$$

or

$$\mu \frac{d}{d\mu} D_0 = M^3 (C_0)^4 \frac{4\pi - 3\sqrt{3}}{4\pi^3}, \quad (31)$$

where the limit $D \rightarrow 3$ has been taken.⁴ This has the form of Eq. (27).

Equation (30) is trivially integrated to find $D_0(\mu)$:

$$D_0(\mu) = D_0(1/a_s) + M^3 (C_0)^4 \frac{4\pi - 3\sqrt{3}}{4\pi^3} \ln(a_s \mu), \quad (32)$$

where we have chosen our reference scale to be the natural s -wave scattering length a_s . Changes in the renormalization scale μ correspond to changes in how well the scattering

⁴Note that there are other diagrams contributing to $[\mathcal{T}_{3 \rightarrow 3}]_{\text{finite}}$. These diagrams, however, have no log divergences and consequently no μ dependence.

at short distances is resolved. As less of the successive two-body scatterings in Fig. (4) is resolved, the contributions are shifted to the three-body contact term D_0 .

We can now use Eq. (32) to obtain the contribution of order $k_F^9 \ln k_F$ to the energy density of the dilute Fermi gas. In order to obtain the full contribution at $\mathcal{O}(k_F^9)$, we would have to renormalize the $3 \rightarrow 3$ amplitude in free space, perform the matching to determine $D_0(1/a_s)$ and then calculate all the energy diagrams at this order. (Alternatively, we could perform the matching with data from a many-body system.) To obtain just the nonanalytic contribution at this order, however, we have only to calculate diagram (k) in Fig. 3, since the logarithm in Eq. (32) must match to the $\ln k_F$ from diagram (l) (plus others) [20]. Equivalently, we keep only Fig. 3(k) with D_0 evaluated at $\mu = k_F$, which avoids large cancellations between the diagrams. Applying the Feynman rules from the previous section we then have

$$\mathcal{E}_4^{\ln} = \rho (g-2)(g-1) \frac{k_F^2}{2M} \frac{16}{27\pi^3} (4\pi - 3\sqrt{3}) (k_F a_s)^4 \ln(k_F a_s), \quad (33)$$

which is the result obtained previously [8–10]. Note that more than a two-fold degeneracy ($g > 2$) is needed to get a non-zero contribution, which follows from Pauli principle restrictions. This procedure can be continued to higher orders to identify further $(\ln k_F)^n$ terms.

V. DISCUSSION AND SUMMARY

We have derived the energy per particle in a dilute Fermi gas through terms of order $k_F^6 \ln k_F$, reproducing results given in Refs. [8–10]. This calculation illustrates many of the virtues of an EFT approach to many-body physics. The EFT provides a model independent description of finite density observables in terms of parameters that can be fixed from free-space scattering with no off-shell ambiguities. Since the system is probed at low resolution, all vertices are contact interactions, which means exchange contributions are trivial and many diagrams vanish. After taking advantage of our freedom to choose a subtraction scheme, the power counting is exceptionally clean: each diagram contributes to a single, well-defined order in the low-density expansion. Finally, the EFT provides tools for identifying and understanding the analytic structure of observables in terms of the short- (and long-) distance behavior. Future extensions of this work will include the generalization to finite temperature, single-particle properties, and linear response, as well as the completed renormalization [7].

One can compare the clean, minimal calculation using an EFT to previous calculations, which required a more general set of diagrams that needed to be summed and expanded, with care taken to avoid double counting. In the standard treatments [8–10], the focus is on the potential, rather than on observables as in the EFT. The EFT perspective says directly that at low energy the effective range parameters matter and not the details of a potential. A corollary is that one can use any complete set of regularized local interactions that reproduces the low-energy observables; there is no “best” potential. It’s not that interactions *are* pointlike at low resolution, but that true observables are *indistinguishable* (up to a well-defined truncation error) from those calculated with pointlike interactions. These interactions are wrong at short distances, but renormalization theory prescribes how

the discrepancy from incorrect high energy behavior can be systematically corrected by the renormalization of the EFT coefficients.

The idea of replacing the “true” potential with one that sums low-energy scattering effects and is easier to work with (a “pseudo-potential”) is an old idea [21]. The EFT framework makes it systematic and extendable. Even if we *did* know the underlying interaction (e.g., a hard sphere potential), it is simpler and more efficient to match in free space to an EFT and then to use the EFT for the finite density calculation. This is analogous to the use of effective theories for heavy-quark physics (NRQCD) and QED bound states (NRQED), which are beneficial even though the underlying theories are known (cf. Ref. [1]).

The EFT analysis can also clarify the nature of many-body systems. In Ref. [13], the energy expansion for a dilute Fermi gas is followed by a discussion of the hole-line expansion, which is used to do a form of power counting. The simple argument is that each additional hole-line is accompanied by momenta restricted by k_F , leading to an additional factor of density that suppresses the diagram at low density. Particle lines have unrestricted momenta and therefore not suppressed, and so must be included to all orders. The power counting in our EFT reveals that a hole-line expansion for the low-density natural Fermi gas is only an artifact of a subtraction scheme that does not remove power divergences. Indeed, the particle-particle and particle-hole ring diagrams in Fig. 3 contribute to the same order in k_F and are numerically comparable. This is cleanly reproduced in the EFT because of minimal subtraction, which results in no distinction between particle and hole lines in the power counting.

We saw that going further in the dilute Fermi gas energy expansion requires input from three-to-three scattering (or other many-body observables). This means that three-body (and four-body) contributions are *inevitable*. If only two-body potentials were used, one would find different results at this order in the expansion for different potentials that agreed for two-body scattering, which would conventionally be attributed to a lack of knowledge of the off-shell two-body potential. From the EFT perspective, the differences would be due to short-distance behavior that must be corrected with many-body counterterms. For the three-nucleon system, accounting for the three-body contact interaction leads to a compelling explanation of the Phillips line [22]. The need to renormalize because of incorrect high-energy behavior is not avoided because of finite loop integrals (e.g., due to a form factor). A sensitivity to cutoff parameters is a signature that something is missing in the theory.

The extension of the EFT procedure for dilute, repulsive Fermi systems to the nuclear matter problem [23,24] is far from immediate. In particular, the EFT subtraction and renormalization scheme used here is not appropriate for a treatment of nuclear matter. That is because the EFT momentum breakdown scale will be set by the lowest mass scale in the effective range expansion, which is of order 10 MeV because of the fine-tuned scattering lengths. Alternative power counting schemes have been proposed to deal with this problem [4,5]. The consistent extension of such a scheme to finite density, which may reintroduce a hole-line expansion, is the next step. However, since nuclear matter equilibrium density is around $k_F \approx 270$ MeV, an EFT with only short-range interactions will still fall far short, with a breakdown scale of $m_\pi/2$ [24]. Thus, pions will have to be included as long-range physics. We are confident that the virtues of the EFT methods illustrated for a much simpler system here will continue to pay dividends as they are adapted to the study of nuclear matter.

Acknowledgements

We acknowledge useful discussions with E. Braaten, J. Ho, G. P. Lepage, R. J. Perry, B. D. Serot, J. V. Steele and N. Tiefessa. This work was supported by the National Science Foundation under Grant No. PHY-9800964. HWH thanks the Institut für Kernphysik at the University of Mainz for its hospitality during completion of this work.

REFERENCES

- [1] G. P. Lepage, “What is Renormalization?”, in *From Actions to Answers* (TASI-89), edited by T. DeGrand and D. Toussaint (World Scientific, Singapore, 1989); “How to Renormalize the Schrödinger Equation”, [[nucl-th/9706029](#)].
- [2] D.B. Kaplan, [[nucl-th/9506035](#)].
- [3] H. Georgi, Ann. Rev. Nucl. Part. Sci. **43** (1993) 209.
- [4] Proceedings of the Joint Caltech/INT Workshop: *Nuclear Physics with Effective Field Theory*, ed. R. Seki, U. van Kolck, and M.J. Savage (World Scientific, 1998).
- [5] Proceedings of the INT Workshop: *Nuclear Physics with Effective Field Theory II*, ed. P.F. Bedaque, M.J. Savage, R. Seki, and U. van Kolck (World Scientific, 2000).
- [6] B. DeMarco and D. S. Jin, Science **285** (1999) 1703.
- [7] H.-W. Hammer and R. J. Furnstahl, in preparation.
- [8] V. N. Efimov and M. Ya. Amusya, Sov. Phys. JETP **20** (1965) 388; M. Ya. Amusia and V. N. Efimov, Ann. Phys. (NY) **47** (1968) 377.
- [9] G. A. Baker, Rev. Mod. Phys. **43** (1971) 479.
- [10] R. F. Bishop, Ann. Phys. (NY) **77** (1973) 106.
- [11] W. Lenz, Z. Phys. **56** (1929) 778.
- [12] K. Huang and C.N. Yang, Phys. Rev. **105** (1957) 767; T.D. Lee and C.N. Yang, Phys. Rev. **105** (1957) 1119.
- [13] A. L. Fetter and J. D. Walecka, *Quantum Theory of Many-Particle Systems* (McGraw-Hill, New York, 1971).
- [14] J. W. Negele and H. Orland, *Quantum Many-Particle Systems* (Addison-Wesley, New York, 1988).
- [15] *Renormalization, from Lorentz to Landau (and Beyond)*, ed. L. M. Brown (Springer-Verlag, New York, 1993).
- [16] R. J. Furnstahl, J. V. Steele, and N. Tiffessa, Nucl. Phys. **A**, in press [[nucl-th/9910048](#)].
- [17] D.B. Kaplan, in Ref. [4].
- [18] E. Braaten and A. Nieto, Phys. Rev. B **55** (1997) 8090; **56** (1997) 14745.
- [19] U. van Kolck, Prog. Part. Nucl. Phys. **43** (1999) 337.
- [20] E. Braaten and A. Nieto, Phys. Rev. D **51** (1995) 6990.
- [21] H.A. Bethe and R. Peierls, Proc. Roy. Soc. A **148** (1935) 146; **149** (1935) 176; G. Breit, Phys. Rev. **71** (1947) 215.
- [22] P.F. Bedaque, H.-W. Hammer, and U. van Kolck, Nucl. Phys. **A646** (1999) 444; Phys. Rev. Lett **82** (1999) 463.
- [23] B. Lynn, Nucl. Phys. B **402** (1993) 281; M. Lutz, Nucl. Phys. **A642** (1998) 171c; [[nucl-th/9906045](#)]; M. Lutz, B. Friman, and C. Appel, Phys. Lett. B **474** (2000) 7; B. Krippa, [[hep-ph/9901212](#)].
- [24] J.V. Steele and R.J. Furnstahl, Nucl. Phys. **A663** (2000) 999c.